Cairo University

Faculty of Engineering

Systems and Biomedical Engineering Department

Diffusion Tensor Imaging

Abdelrahman Alaa
Adham Khaled
Anas Mohammad
Eman Emad
Farha Sayed
Rawan Shoeib

Supervisor: Professor Mina Makary

June 26, 2025

Contents

List of Figures

Abstract

This work explores the principles and applications of Diffusion Tensor Imaging (DTI) in modern medical diagnostics. Since DTI works by using the regular Magnetic Resonance Machine with some modifications to tag the diffused water molecule, we first dedicate a chapter to review the fundamental mathematics and physics of Magnetic Resonance Imaging (MRI), how MR images are constructed, T1 and T2* signals and other key topics.We then discuss the basics of diffusion measurement process and how to monitor water diffusion using the normal MR images. The next chapters are dedicated to the DTI itself with a focus on the pervious work, The process of tensor imaging in detail, modern applications, a case study and how DTI compares to other imaging modalities.

Keywords: Diffusion Tensor Imaging, Diffusion Kurtosis Imaging, Magnetic Resonance Imaging, MRI, DTI, DKI, Medical Imaging, Neuro imaging, Brain Science

Chapter 1

Literature Review

Advanced MRI techniques have greatly helped us study the detailed structure and connections of the human brain non-invasively. Among these, diffusion tensor imaging (DTI) has been a powerful tool for mapping the brain's neuro anatomic connectome. The potential of DTI to provide rich information about white matter pathways quickly established it as a cornerstone of brain research and an increasingly valuable asset in clinical practice.

The birth of water diffusion MRI can be traced back to the mid-1980s when Denis Le Bihan, driven by the challenge of differentiating liver tumors from angiomas, conceived the idea of mapping water molecular diffusion coefficients in tissues in vivo. Drawing upon the pioneering work of physicists like Stejskal and Tanner in the 1960s on encoding diffusion using magnetic field gradients, Le Bihan successfully integrated these gradients with MRI scanner technology. His initial trials on the liver were hampered by motion artifacts, leading him to shift his focus to the brain. The world's first diffusion images of the brain, made public in 1985, demonstrated the significant neurological potential of this new technique per. Le Bihan also recognized that water diffusion in tissues differed from free water diffusion, leading to the concept of the Apparent Diffusion Coefficient (ADC) to describe these findings.

Early explorations with diffusion MRI revealed a crucial characteristic of water movement in white matter: its anisotropic nature. Researchers observed that water molecules diffused much more readily along the direction of nerve fibers than across them as in Sakuma et al. (1991). Shortly thereafter, Michael Moseley in Moseley et al. (1990) at UCSF made an unexpected but crucial discovery in an acute cat brain ischemia model: Water diffusion dropped significantly (30–50%) during the very early phase of acute brain ischemia. This finding highlighted the sensitivity of diffusion MRI to acute pathological changes in the brain.

Building upon these foundational discoveries, Peter Basser and Denis Le Bihan in Basser et al. (1994), along with their colleagues, embarked on the development of Diffusion Tensor Imaging (DTI) in the mid-1990s. DTI aimed to quantify this directional dependence of water diffusion, or diffusion anisotropy, by employing tensor mathematics as in Basser (1995) and Basser and Pierpaoli (1998). Following its establishment, DTI experienced rapid adoption within the neuroscience community. The fact that over 700 research papers using DTI were published by 2007 as Assaf and Pasternak (2007), not long after the technique was established, clearly shows how quickly it became a vital tool in brain research.

To capture this anisotropy, DTI involves acquiring diffusion-weighted images with gradients applied in multiple non-collinear directions. By employing tensor decomposition, this tech-

nique allows for the extraction of the principal diffusivities: axial diffusivity ($\lambda//$), representing diffusion along the fibers, and radial diffusivity ($\lambda \perp$), representing diffusion perpendicular to them. From these fundamental measures, various scalar indices have been derived to characterize the properties of water diffusion within each imaging voxel. Among these, the trace of the apparent diffusion coefficient (trADC) or mean diffusivity (MD), which reflects the overall magnitude of diffusion, and fractional anisotropy (FA), a normalized measure of the degree of directional preference in diffusion, have become particularly prominent. While numerous other diffusivity-based metrics have been proposed over time as in Basser and Pierpaoli (1996), Papadakis et al. (1999) and Westin et al. (2002), FA quickly established itself as the most widely adopted index in brain research, providing a grayscale representation of diffusion anisotropy that effectively highlights white matter pathways per Pierpaoli et al. (1996).

A significant strength of DTI lies in its rotational invariance, enabling it to measure the main ways water moves and their 3D direction within brain fibers, regardless of how those fibers are oriented in space. This directional information not only allows for quantitative analysis of diffusion anisotropy but also for the visualization of white matter architecture through color-coded maps, most notably the red-green-blue (RGB) scheme, which assigns colors based on the primary fiber orientation within each voxel as per Pajevic and Pierpaoli (1999). Furthermore, the directional information inherent in DTI data paved the way for tractography techniques, which reconstruct virtual pathways of white matter fiber bundles by following the principal diffusion direction, offering wonderful insights into the brain's anatomical connectivity. This capability moved MRI into the area of studying neural connections in vivo, a domain previously limited to invasive histological methods.

Radiologically, DTI has provided a novel contrast mechanism in MRI, with FA maps effectively outlining white matter structures due to their high anisotropy compared to gray matter and cerebrospinal fluid. This has proven particularly useful in visualizing white matter surrounding brain tumors, where fibers can be displaced or infiltrated, helping in presurgical planning and patient management as per Witwer et al. (2002), Assaf et al. (2003) and Clark et al. (2003). While its application in other neurological and psychiatric disorders can be a bit more complicated, DTI has contributed to the investigation of white matter abnormalities in conditions like schizophrenia, Alzheimer's disease, and multiple sclerosis per Catani and ffytche (2005), Kanaan et al. (2005) and Bozzali (2002) .

Despite the significant advancements offered by DTI, the underlying model rests on certain assumptions that may not always accurately reflect the complex reality of brain tissue. The assumption that water diffusion follows a Gaussian distribution has been challenged by findings indicating non-Gaussian behavior due to restricted diffusion within the intricate cellular environment as in Assaf and Cohen (2000), Assaf and Basser (2005) and Jensen et al. (2005). Furthermore, the representation of each imaging voxel, containing a big number of axons and glial cells, by a single diffusion tensor is a simplification that can lead to inaccuracies, especially in regions with complex fiber architecture or partial volume effects per Papadakis et al. (2002).

To address these limitations, more advanced diffusion MRI techniques have appeared. Diffusion kurtosis imaging (DKI), pioneered by Jensen and colleagues in the mid-2000s, represents a significant step beyond the Gaussian diffusion assumption of DTI. DKI employs a higher-order diffusion model that not only considers the diffusion tensor but also incorporates kurtosis, a measure of the deviation of the diffusion profile from a Gaussian shape. This additional parameter, kurtosis (Kapp), is sensitive to the complexity of the tissue microstructure

and can potentially reveal information about cellular heterogeneity and barriers to diffusion that are not captured by DTI. While initially applied primarily in brain imaging, DKI is increasingly being explored for its potential in various clinical applications such as improved tumor detection and grading in the prostate, assessment of head and neck cancers, evaluation of breast diseases, and investigation of lung and kidney tissues.

The development of DKI and other advanced diffusion MRI techniques signifies an ongoing effort to overcome the inherent limitations of DTI and to provide a more accurate and comprehensive characterization of brain microstructure and connectivity. While DTI remains a powerful and widely used tool, these evolving methodologies offer the potential for further advancements in our capacity to investigate the characteristics of the human brain in both health and disease.

Chapter 2

Magnetic Resonance Imaging Basics

2.1 The Source of the MRI Signal

2.1.1 Quantum Spin and Electromagnetism

The idea behind using the MRI machine is to obtain a signal that can be used to build a 3D model of the human body. The MRI signal obtained is mainly the electromagnetic response emitted from free protons found in the water molecules when subjected to an external magnetic field.

To understand how the MRI signal is generated we have to be familiar with a property of matter called the quantum spin. The quantum spin is a fundamental property of matter just like mass and charge. The nucleus of the matter consists of protons and neutrons. Protons and Neutrons are actually made up of fundamental particles called quarks. Quarks come in 6 types and it is quarks actually what give matter the quantum nature and hence quantum properties as spin. Although the name may imply the presence of rotation, spin is not an actual physical rotation. To understand the magnetic properties of a proton, we can think of the quantum spin it as an internal invisible angular momentum that will make the proton behave as it is actually rotating.

We also have to be aware that laws of electromagnetism state that a charged particle in motion produces a magnetic field and specifically if that charged particle is in circular motion as in a coil for instance, it induces a magnetic filed similar to that of the bar magnet in Fig.2.1 where inside the bar magnetic field lines flow from south to north then from the north flows radially outward towards the south again.

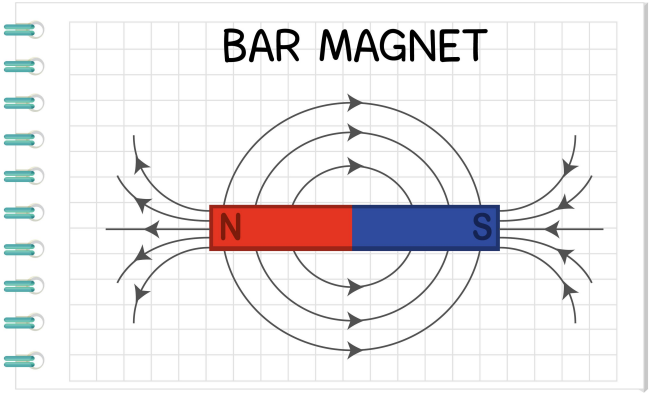

Figure 2.1: Bar Magnet Magnetic Field Lines

2.1.2 Protons as Tiny Bar Magnets

Now since a proton is a charged particle and behaves as if it is **internally** spinning or precessing due to its quantum spin it will produce a magnetic moment denoted as μ that is a function of the quantum spin:

$$\hat{\mu} = \gamma \hat{S} \tag{2.1}$$

S is the quantum spin vector and γ is a constant ration between the Magnetic moment and Quantum Spin called the **gyromagnetic ratio**. The magnetic moment μ is a vector that describes the intensity and direction of how much the proton behaves like a **compass magnetic needle** or how it will respond to an external magnetic field. The magnetic moment of a compass needle is what makes it respond to external fields like that of Earth. Furthermore, this moment is what give the needle its own magnetic field that have that have its flux lines flowing between north and south as a bar magnet. The magnetic field vector direction is typically represented by the north vector direction as in the following Fig:

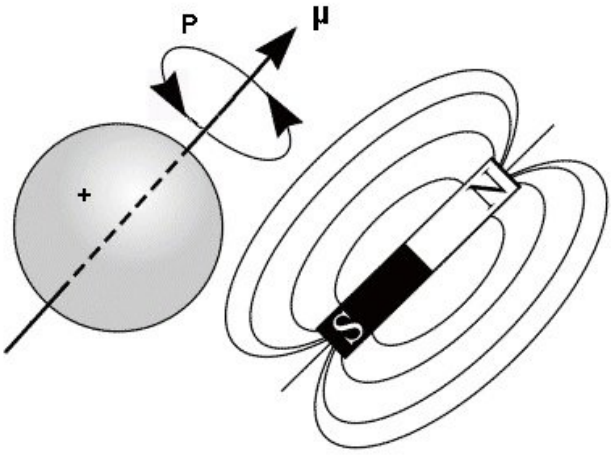

Figure 2.2: Proton Actins as a Magnet Bar

2.1.3 Free Induction Decay

The magnetic field generated by the protons will be the source of the MRI signal in its most raw form. This raw form is no more an induced alternating voltage signal due to the changes in

the magnetic field of the protons. The voltage signal is detected by coils in the MRI machine according to Faraday's Law of Induction,

$$\epsilon = -\frac{d\phi}{dt} \tag{2.2}$$

ϵ is the induced voltage and ϕ is the magnetic field lines intersecting with the machine coils. This voltage signal is called the **Free Induction Decay** and by processing this analog voltage signal we will be able to extract the required information to produce an image.

2.1.4 Protons Wobbling Rotation and Larmor Frequency

When a patient is in the MRI machine, the Z-axis will be directed longitudinally along his body, the x-axis will span from the his right arm to his left arm, and the y-axis will represent the vertical direction as shown in Fig.2.3.

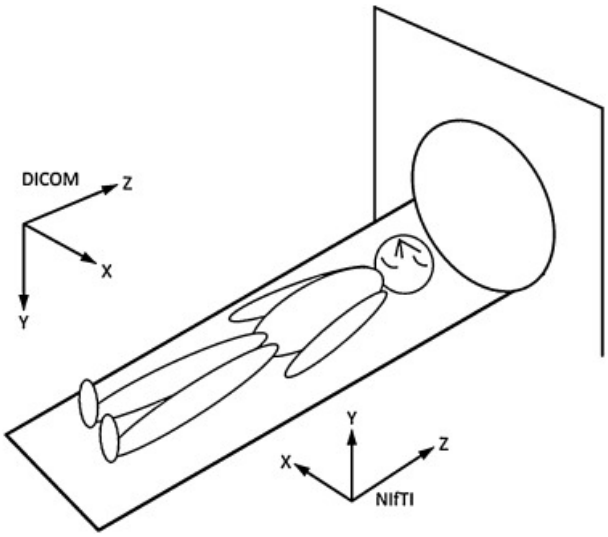

Figure 2.3: MRI Axes Orientation

Under normal conditions the protons magnetic moment vector directions in the human body are randomly oriented so there is not a net magnetic field vector. The MRI machine applies a strong magnetic field denoted as B_0 that will be pointing towards the $+$Z direction and hence all the protons magnetic moments vectors will either align with Bo or in its exact opposite direction with a few more aligning with B_0 resulting in a net magnetic field vector aligning with B_0 as shown in the following figure:

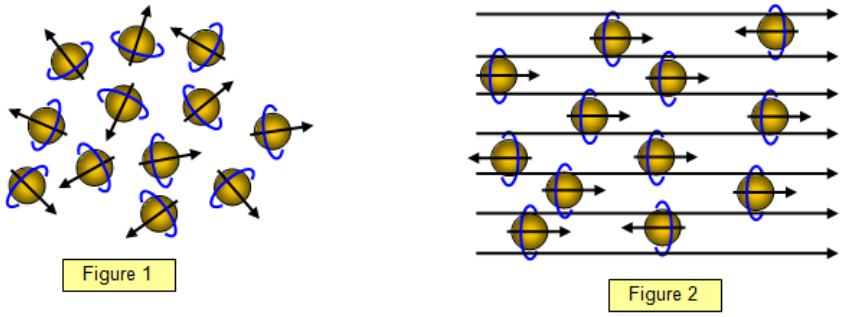

Figure 2.4: Effect of External Field on Protons Magnetic Field
image from Exchange (2019)

The fact the some protons align with negative direction of B_0 is due to the internal excitation states of the hydrogen atoms, but the most important here for our imaging process that the field vector are aligned along the Z-axis whether positive or negative.

When Protons magnetic moments are forced to align with the huge MRI external field they won't be completely aligning with B_o but will be actually wobbling around the B_0 direction as shown in Figure 2.6.

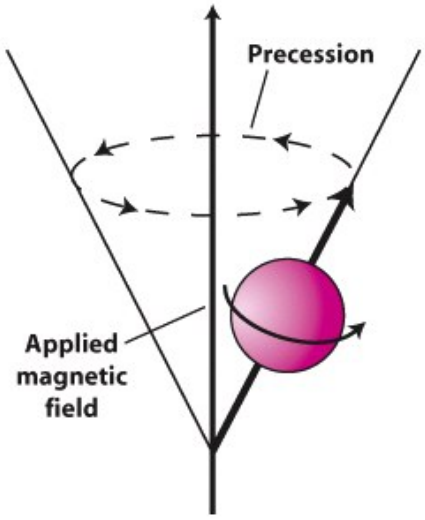

Figure 2.5: Proton wobbling around the B_0 field direction (Larmor precession)
image from Duke University (2023).

The wobbling behavior arises because of the proton own magnetic field. Interestingly, the quantum spin again mimics an actual physical rotation making the magnetic moment vector behave as if it was rotating so when this "rotating" vector is forced to align with the much stronger B_0 the rotation will be a resistance to the pulling force of B_0 causing the wobbling behavior. This can be visualized by the example of the spinning top when it is angular momentum is decaying it does not stop rotation in its exact place but rather its rotation resists the Earth gravity vector that is passing through the top center causing its wobbling around the gravity vector as shown in the following figure:

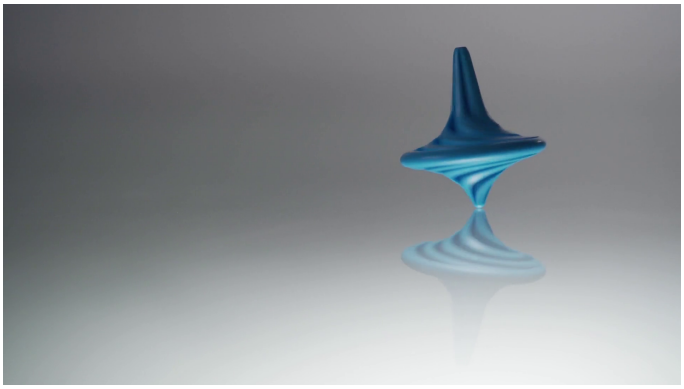

Figure 2.6: Spinning Top Wobbling.

But Why does not the the protons stop wobbling as the top does thought? Again because its wobbling is due to the magnetic moment rising from the quantum spin that is an inherent property just as the proton charge which means it exists as long as the proton exists or until the external field diminishes. The wobbling rotation frequency is defined by a unique frequency called **Larmor Frequency**. The equation defining this frequency is:

$$\omega = -\gamma B \tag{2.3}$$

where B is the external field that will be B_0 in our case and gamma is a constant called the **Gyromagnetic Ratio**. Now the wobbling magnetic moment of the proton can be decomposed into two vectors: a longitudinal one along the Z-axis aligned with Bo that contributes the most to the magnitude and direction of the magnetic moment and another transverse component rotating in the XY plan with the Larmor Frequency.

2.2 Slicing along the Z-Axis

2.2.1 Slice Selection

The 3D model made by the MRI machine is actually constructed by imaging the body in 2D slices along Z-axis and stacking them together to create a 3D model. In order to be able to choose which slice to image, we should be able to control which hydrogen protons will respond the imaging procedure and this is done by applying a **Magnetic Field Gradient** denoted as G_z along the z-axis. G_z, measured in $Tesla/m$, will vary linearly with z such that the magnetic field magnitude at each z-position is $B_0 + (z * G_z)$. That will make each slice along the body have its protons precessing at a different **Larmor** Frequency. So to choose a specific slice we should apply an oscillating magnetic field denoted $B1$ with that slice's Larmor Frequency that will select that slice since the Larmor frequency here resembles the resonance frequency.

The coils that will detect the **Free Induction Decay** caused by the change in the magnetic fields of protons are positioned such that they will induce current upon field changes in the XY plane only. So to get a signal, the protons magnetic moment must have a component in the XY plane and hence the applied $B1$ should be able to tip some or most of the magnetic moments to be oriented in the transverse XY plan. The net magnetization vector caused by the summation of all protons fields components in the XY plan will be denoted as M_{xy}. The following figure shows the section process.

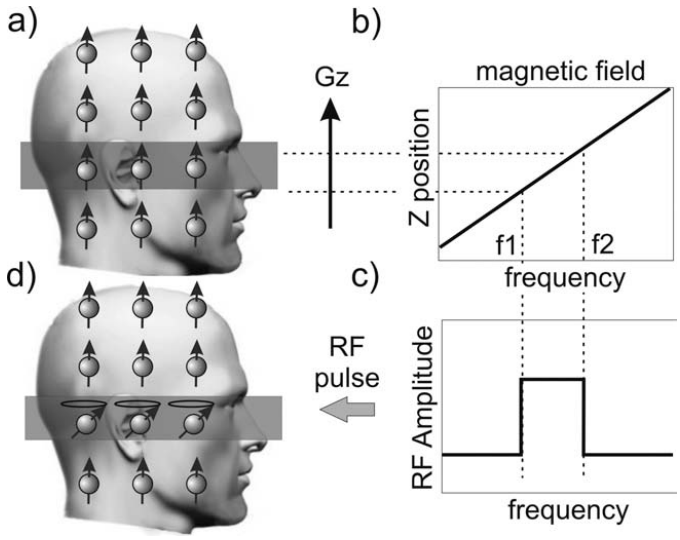

Figure 2.7: Effect of Applying an Electromagnetic Pulse Orthogonal to the Gradient Magnetic Field)
image from MATLAB1 (2023).

2.2.2 Obtaining Magnetization in the Transverse Plan

To obtain M_{xy} , $B1$ will be that of a radio frequency (RF) wave pulse magnetic field denoted applied in the transverse plan. Radio waves are electromagnetic waves and hence their magnetic field vector direction is oscillating. When the RF pulse field is applied in the transverse or XY plane it means that its vector direction will be rotating in the XY plan with the Larmor Frequency of the desired slice. An external field applied for a period t on a magnetic moment with angular momentum like that of the proton μ will cause a torque that is dependent on the angle between them and hence the magnitude of the torque on μ around B1 axis can be calculated as :

$$||\tau|| = ||\mu X B1|| \tag{2.4}$$

that will cause μ to rotate with an angle :

$$\alpha = \gamma B_1 t \tag{2.5}$$

By looking at Fig.2.6, we can see the wobbling moment vector can be decomposed to components. The first is a longitudinal static component aligned with Z-axis or B_o and that component is one dominating the moment vector direction and magnitude. The other component will be a rotating vector with the Larmor Frequency in the XY plan.

Lets now consider what will happen to each component when we apply the RF pulse. To simplify the visualization process we will assume the rotating frame of reference and assume that the XY plan is rotating around the Z-axis. Lets call the rotating transverse plan X'Y' plan and assume the RF pulse is applied along X'. Its rotating field vector in the normal frame of reference will appear static from a rotating reference. According to equation2.4 this will exert torque on the longitudinal components pulling them towards its direction of action. But since the pulled longitudinal component has its own angular momentum from the quantum spin property the longitudinal components will rather trace a decaying spiral around the X' until it converges to wobble around it.

According to equation2.5, if the RF pulse was applied for a period t = $90/(\gamma B_1)$ we can tip the longitudinal components with 90 degrees so that they will almost point along the Y‘. For the transverse components, they will also be tipped by 90 but they will also be synced to have the same phase. So now we have M_xy from the longitudinal components and from the contribution of the transverse components once they have been synced together and rotating with Larmor Frequency. Since that RF pulse has tipped the magnetization from Z to XY it is called the 90 RF pulse.

2.3 Circular Frequency Nature of Protons Magnetic Fields and Quadrature Coils

2.3.1 Frequency Complex Representation

Now that we have a component of the magnetic field in the XY plan it is suitable to discuss now the composition of the FID signal and the nature of their receiving coils. Imagine a single frequency ω with phase ϕ and amplitude R. This frequency component can be formulated as a simple sinusoidal as R$cos(\omega t + \phi)$. This is usually is sufficient but it suggest that the frequency component is made of only a real part where the general complex representation for a frequency component is R$cos(\omega t + \phi)$ -$jRsin(\omega t + \phi)$ or $Re^{-j\omega t+\phi}$.

The complex or the Euler representation of the frequency includes the whole information it carries relative to the 2D complex plane and any of those two representation if plotted on the complex plane will represent a vector starting from $\theta = \phi$ and drawing a circle of Radius R. In that way the frequency induced in the coil can be though of as more of a circular frequency or a frequency that originates from a circular motion which is true since each proton magnetic field is actually wobbling or rotating in the space tracing a circle around B_0.

2.3.2 Quadrate Coils

Now that we know the nature of the signals frequencies emitted from the protons, it is convenient to use a type of coil that will receive the circular nature of that frequency or in other words induces a complex signal. This is way coils the FID signals will be induced in are **Quadrature Coils**. It consists of two regular coils positioned to be perpendicular to each other. A very simple illustration is shown in Fig.2.8. Since sine and cosine are orthogonal to each other in the complex space any signal induced in the quadrature coil will be decomposed into a real cosine and imaginary sin components.

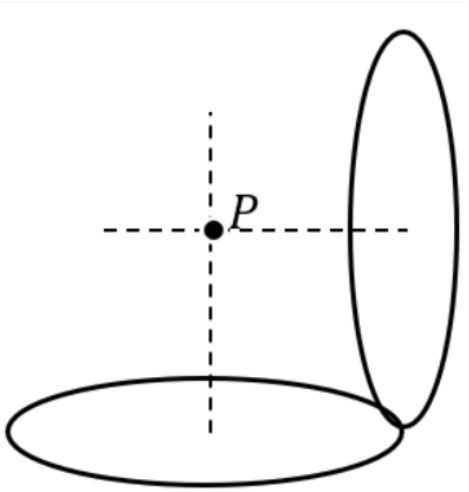

Figure 2.8: Quadrature Coils

2.4 FID Signal Reading and Processing

2.4.1 Composing the FID Signal

After the RF pulse has been applied and there is no longer a driving force for protons magnetic fields to be oriented orthogonal to the Z-axis, their moment vector will begin decaying from completely orthogonal to the z-axis until they reach their original state of wobbling around the z-axis and hence the M_{xy} is going to decay gradually. Another procedure to be applied is the spatial encoding of the x and y coordinates of the protons. Since all protons per slice are precessing at the same frequency and phase we are not able to extract spatial information from the FID signal. It means that we won't know which protons along the X and Y axis have contributed more to the signal.

2.4.2 Spatial Encoding across the XY Plan

Therefore, just as the protons fields begin to decay, a gradient magnetic field G_y is applied for a very brief time interval τ in the Y direction. Now the total magnetic field at position y will be $B_0 + yG_y$ forcing protons to precess at different different Larmor Frequencies similar to what happened with G_z. However, G_y was not intended to change frequencies since it was applied for a very short time. So, protons will return to precess at the same frequency again after it ceases to exist. It will however cause the protons to dephase or precess at different phases.

This happens due to the natural relation between frequency and phase. Frequency is no more the than the cycles completed per second to return to the same phase point again. For example, a clock cycle would be going from 12 am to 12 am the next day and hence phase is defined as the accumulation of a certain frequency for a certain period of time. The following equation describes that relation:

$$\phi = \int_0^{\tau} \omega(t) dt \tag{2.6}$$

where ϕ is the final or "locked" phase with the proton after a certain frequency ceases to exist and τ is the life time of that frequency. Before the application of G_y the Larmor frequency ω_0 of each proton was defined by the equation 2.3 and since the frequency is constant the phase ϕ will always be constant and equal to $\int_0^t \omega_0 dt = \omega t$ where t is the time from the beginning of the scan until G_y is applied. While G_y is applied for the period τ the total Larmor Frequency according to equations 2.3 and 2.6 will be deduced as follows:

$$\omega = \gamma(B_o + yG_y) = \gamma B_0 + \gamma y Gy = \omega_0 + \gamma y Gy \tag{2.7}$$

so the new frequency will be just the original frequency added to the frequency resulting from the field gradient.After the G_y diminishes the phase that will be locked with the protons can be calculated as:

$$\phi = \int_0^\tau (\omega_o + \gamma y G_y) dt = \omega\tau + \gamma y G_y \tau = \phi_c + \phi_y \tag{2.8}$$

That resulting phase will be trapped with the protons even after the frequency causing it diminishes so now the phase of all protons will have a new phase depending on the y-position of the protons and especially the term ϕ_y since ϕ_c will not cause variability. Now all protons are precessing at the original frequency ω_o but are not in phase.

Let us remember that G_y was applied just after the RF pulse has been applied so now we are in the interval when protons are decaying back to the Z-axis with the same frequency but with different phases and hence the FID is already being induced in the coils. As the signal is read out, a field gradient X G_x measured in T/m just like G_y and G_z along the X-axis but this time the field will be permanent until the next readout (When there is no more signal and protons have already returned to wobble around the Z-axis). Therefore, at each x position, the total field will be $B_0 + xGx$ and according to equation 2.3 each proton will be precessing with a different frequency:

$$\omega = \gamma(B_o + xG_x) = \gamma B_0 + \gamma x G_x = \omega_o + \omega_x \tag{2.9}$$

. So the total frequency will be just the original Larmor frequency plus the frequency due to the G_x.

2.4.3 FID signal in its Final Form

Remember that we stated the Euler representation $Re^{-j\omega t+\phi}$ will be used to describe the voltage signal induced from changes of the magnetic field of each proton. We have now identified how the frequency and the phase will be produced so are left with the R or the magnitude of the signal. The magnitude of the signal will be naturally the magnetization M_{xy}. Now using equations 2.3, 2.9 and 2.6, the FID can be formulated as following:

$$V(t) = \int_0^{D_y}\int_0^{D_x} M(x,y)e^{-j[(\omega_o+\omega_x)t+\phi_c+\phi_y]}dxdy = \int_0^{D_y}\int_0^{D_x} M(x,y)e^{-j\omega_o t}.e^{-j\omega_x t}.e^{\phi_c}.e^{\phi_y}dxdy \tag{2.10}$$

where Dx and Dy are the width and the height of the slice. To simplify calculations we can scale the signal and omit the term e^{ϕ_c} since it does not depend on x, y or t. The term $e^{-j\omega_o t}$ is also a constant term relative to the integral and is a mutual contribution from all protons that can be accounted for at the end, so processing techniques perform demodulation to remove it so that we are only left with terms dependent on the spatial dimensions. The equation then simplifies to :

$$\int_0^{D_y} \int_0^{D_x} M(x,y) e^{-j\omega_x t} . e^{\phi_y} dx dy \tag{2.11}$$

2.5 T Signals

2.5.1 T2 and T2*

So how do we get to differentiate between different tissues? In other words, how will different details be visible in the MRI image? Even when protons are subjected to the same external field, they can grow slightly out of phase from each other. Since protons in the water molecules are naturally extremely close to each other, they act as tiny external fields on each other that is a property know as **spin to spin interaction** causing the accumulation of phases from time to time. These different phases reduce the total signal M_{xy} causing it to decay over time even if the protons were to stay precessing in the XY plan and not realign with the Z-axis.

This is why the MRI FID signal decay caused by the spin to spin interactions is called**T2 decay or T2 signal**. However, T2 effect is almost negligible and that is why we have introduced much stronger dephasing by applying the G_y gradient that will cause the protons to have very different phases and hence cause stronger decay to M_{xy}. The decay caused by T2 plus that caused by the G_y is called **T2* decay**. T2 and T2* are formally defined as the time taken for M_{xy} to be reduced to 37% of the maximum value. In the following figure we can see that logically T2* decays faster than T2 as T2* has stronger dephasing including that of T2.

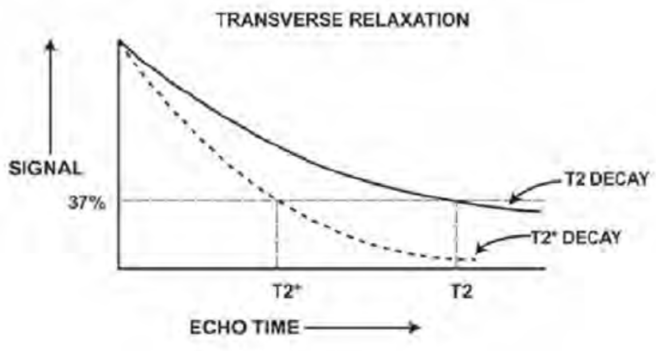

Figure 2.9: T2 and T2* Relaxation

2.5.2 T1 Signal

The other much more obvious decay caused to the M_{xy} and hence to the FID is that caused by the natural decay of the protons to realign with the z-axis casing the magnetic field component in the XY plan to decay over time. This relaxation is rather know as the **T1 Relaxation**. Instead of being defined as the time taken for M_{xy} to decrease to 37& of it maximum, it is defined as time taken for M_z to recover 63% of its maximum value. It is just the other way around as shown in the following figure.

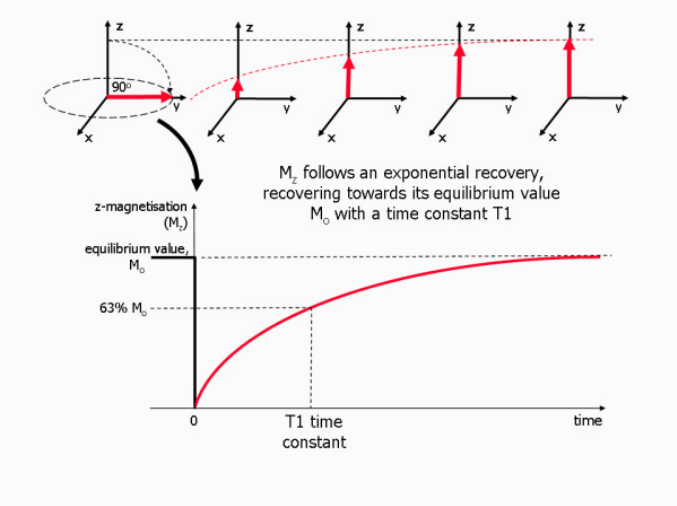

Figure 2.10: T1 Relaxation

2.6 MRI Image Construction

2.6.1 K-Space Map Filling

Remember that the final simplified version of the FID is the equation **??**. From a zoomed out perceptive it looks like a traditional 1D analog complex voltage signal detected in the coils, how can we construct an image from it? By zooming at the equation again we can see that the process of linking the temporal Larmor frequency and its phase with the x and y coordinates made that the formula very close to the 2D Fourier Transform. Recall that $\omega_x = \gamma x G_x$ and $\phi_y = \gamma y G_y \tau$.we can then rewrite the equation as :

$$\int_0^{D_y} \int_0^{D_x} M(x,y) e^{-j\gamma x G_x t} . e^{\gamma y G_y \tau} dx dy \tag{2.12}$$

Let $k_x = \frac{\gamma}{2\pi} G_x t$ and $k_y = \frac{\gamma}{2\pi} G_y \tau$ and plug those in the previous equation and add constants required to maintain the equation as it is we get

$$\int_0^{D_y} \int_0^{D_x} M(x,y) e^{-j2\pi(k_x x + k_y y)} dx dy \tag{2.13}$$

This is actually the formula for the **Continuous 2D Fourier Transform** where k_x and k_y are the two spatial frequency variables. However, It would be very computationally expensive if we perform the double integral across the entire slice surface, so we will sample the slice

across the x and y direction to get discrete and y positions and hence the FID as a **Discrete 2D Fourier Transform** as follows:

$$\Sigma_{y_n=0}^{N_y-1}\Sigma_{x_n=0}^{N_x-1}M(x_n,y_n)e^{-j2\pi(k_x x_n+k_y y_n)} \tag{2.14}$$

N_y and N_x are the number of points taken along the y and x axis respectively.

Now is the final obstacle. By looking at the previous equation one might think it will give the complete Fourier Transform or in other words give a 2D discrete map of dimensions that of the slice scanned. The trick is for the 2D Fourier Transform to completely work the spatial frequency variables k_x and k_y must be evaluated at all the possible values according to the previous equation While they were only evaluated at $k_x = \frac{\gamma}{2\pi}G_x t$ and $k_y = \frac{\gamma}{2\pi}G_y \tau$.

Since that k_x is evaluated at different time instants this previous will actually fill one row of our 2D map where each column correspond to a different t. That is why actually multiple FID readouts are obtained for the single slice or exactly N_y time where each time when the protons have already realigned with B_o, a new RF pulse is applied that resets the protons to precess in phase and with the same frequency. The same G_x is applied but with different G_y so that now k_y is evaluated at a different G_y to fill the next row. We then have a complete 2D Grid of how the Magnetization M_{xy} changes according to the two spatial frequency variables k_s and k_y. This grid is called the **K-Space map**.

Now a simple **2D Inverse Discrete Fourier Transform** will convert the K-Space Map into a gray Image. Now when multiple slices have been obtained along the Z-axis, they are layered upon each other to form the 3D model.

2.6.2 Magnetization M_{xy} Weighting

Finally, we should actually know what causes the magnetization across a slice to change. Magnetization magnitude is affected by the T1 and T2* signals as mentioned before. Different tissues exhibit different T1 and T2* decay waveforms and hence cause the magnetization magnitude to differ across the slice. Although both signals naturally contribute to the overall decay of the M_{xy} we can control which signal we want to focus on and that is why MRI images are classified to T2* weighted images and T1 weighted images.**Repetition Time (TR)** and **Echo Time (TE)** are two key terms that are important to understand how these signals weight the image. TR is the time between between the RF pulses application and TE is the time left after the RF pulse and the application of G_x.

When it comes to T2*-weighted images, long TR time and long TE are applied the long TR is applied so that almost all tissue types have enough time for their protons to fully decay and realign with B_o. This way the max M_z is recovered and the next RF pulse it will be fully tipped to the XY plane. In that sense the effect of T1 signal is not dominant.

Tissues as the cerebrospinal fluid that show weaker spin to spin interactions (T2) allow M_{xy} to decay slower and have a greater magnitude before applying G_x and reading the signal and hence they appear brighter in the gray T2* weighted images. So, to fully account for decay effect of the natural spin to spin interactions and that caused by the G_y a long TE is applied. Although all tissues are subjected to the same G_y, it is main mission was to emphasize the dephasing caused by the natural T2 by causing more different phases and also encode the

y position.

For T1-weighted images, a short TE is applied so that dephasing caused by T2* does not get a chance to affect the magnetization a lot and hence T2* effect is not dominant. For T1 effect to be dominant, a short TR is applied so that the faster a tissue realigns with B_o, the more M_z will recover and hence when the next RF pulse is applied it will have greater field to be tipped in the XY plane and hence appears brighter in the image. Fatty tissues have lower T1 time so they appear bright in T1-weighted image.

Chapter 3

Diffusion Weighted Magnetic Resonance Imaging

3.1 Diffusion Measurement

3.1.1 Types of Water Movements in Human Body

Now that we know to obtain an MRI image, we should investigate how can we apply some adjustments to account for the motion of water molecules inside the human body. As mentioned before, the signal of the MRI is affected by the T1 and T2* signals of different tissues. The number of free protons known as the**proton density** also is a main factor. It just means that more protons will produce more magnetic field changes that will affect how the Free Induction Decay in the coils look like.

Water can flow in the human in body in bulk, in directional flow or via diffusion. Bulk motion is the collective motion of water molecules in the brain due to random motion of patient or due to natural brain pulsations. This type of motion can produce motion artifacts as ghosting or co registration of different brain volumes as shown in the following figure:

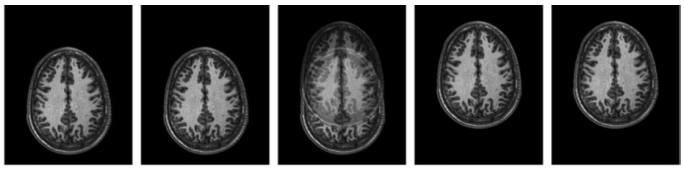

Figure 3.1: Co registration Error Due to Bulk Movement

When it comes to water flow we mean the directional organized movement of water that is typically guided by blood vessels. Both flow and bulk motions are macroscopic types of motions which means both represent collective behavior of many water molecules together.

Diffusion however is microscopic in nature. The driving factor for diffusion is the concentration gradient. Wherever there is a difference between two regions in the number of water molecules, each water molecule is driven individually to fill that gradient gap. Since each water molecule behaves individually, the overall motion of diffused water is random just as a droplet of ink spreads in all direction in a glass of water. Diffusion hence is called the **random motion** and can also be called **Intra Voxel Incoherent Motion (IVIM)**. We now

know why motion is incoherent but the part intra voxel means that when examining an MRI image we investigate how each voxel has been affected by diffusion of water molecules. The same voxel with the same tissues can appear bright in one brain volume while dull in the next brain volume due to diffusion of water from that voxel.

3.1.2 Tagging Water Diffused Molecules

Let us recall that to apply phases changes among the protons we applied the gradient G_y, so at the end of the reading process the protons have all relaxed and are now precessing at the same Larmor frequency but have different phases. To know which water molecules have diffused during the scan a **Re phasing Gradient** $-G_y$ is applied so that it cancels the phasing effect of G_y. If all water molecules were stationary, the reshaping will be perfect returning all protons to be in phase. Protons inside water molecules that have diffused during the scan will have gained more phase than that produced by the G_y and hence some protons will be out of phase and cause decay to the total FID Signal. The extra phase comes from the fact that we have encoded the spatial domain with gradually changing frequencies and phases and hence moving through the domain meaning coming under the effect of multiple frequencies and phase.

Voxels that have these out of phase protons will represent the final destination of diffused water molecules. The following two figures can illustrate the process:

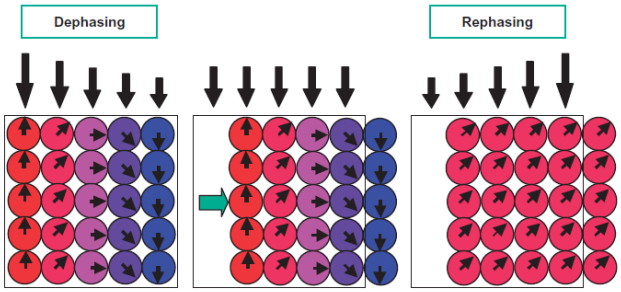

Figure 3.2: Dephasing and Re-phasing Pair Without Water Diffusion

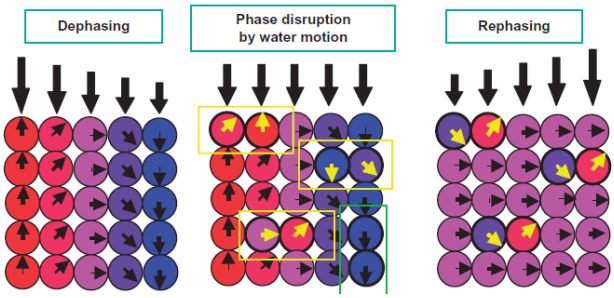

Figure 3.3: Diffusion Effect on the Dephashing-Rephasing Pair

3.2 The Mathematics Behind the Diffusion Measurement

3.2.1 Spin-Echo Sequence

The process of phasing and re-phasing the protons to track the process of diffusion can be challenging if the signal decay caused by T2* star was so much that is caused much dephasing for us to be able to differentiate between T2* induced phases and phases due to diffusion. That is we apply a procedure called the **Spin Echo Sequence** by applying a refocusing 180 RF pulse usually at TE/2 to compensate for the decay caused by T2*.

Like the 90 RF pulse applied to tip the magnetization vector with 90 to be in the XY plane, at the middle of the TE a 180 RF pulse is applied to refocus the signal by inverting the phases of the XY components of the protons magnetic moments. It will also invert the longitudinal relaxing components but the RF interval of application is too short for them to affect the process of the spin echo sequence.

This inverting will make protons rotate in the opposite direction so that previously faster protons are now slower so that all protons catch up forming an echo that represent the total M_{xy} recovered again. The following figure illustrates this operation.

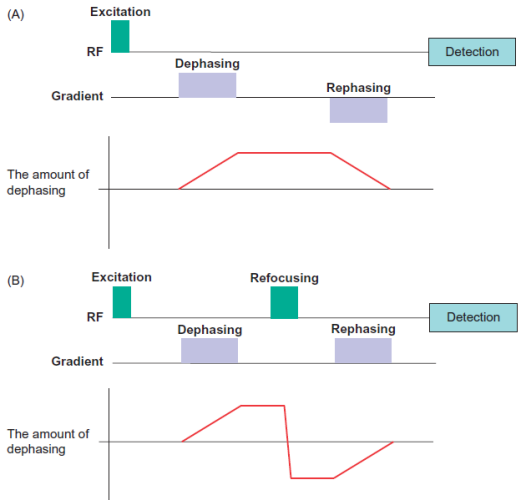

Figure 3.4: Spin-Echo Sequence Procedure

3.2.2 Parameters Affecting Diffusion Measurement

The first and most obvious parameter to affect the Diffusion measurement process is the **Diffusion Constant** D. Tissues with greater Diffusion ability will travel longer distances with the same interval T. T then is itself an affecting parameter because the longer we wait to measure the diffusion the more T2* decays will be dominant. To accurately measure the diffusion constant, we have to perform two experiments. One experiment without the diffusion weighting gradients pair and the other with using them. In that sense we will first obtain a normal T1 and T2* weighted images without the effect of diffusion and from the second experiment we obtain the effect of the diffusion on the images.

3.2.3 Mathematical Description of Diffusion Weighting Experiments

Since we will be depending on two separate signals obtained from two separate experiments to measure diffusion we will define S_o as the signal obtained from the normal MRI imaging experiment and S as the signal obtained from using the diffusion weighting gradients pair. The ration can be formulated as:

$$\frac{S}{S_o} = e^{\gamma^2 G^2 \delta^2 (\Delta - \frac{\delta}{3}) D} \tag{3.1}$$

γ is the gyromagnetic ratio, G is the strength of the phasing or re-phasing gradient, Δ is the time interval between the phasing and re-phasing gradients, δ is the spatial length of the G application and D is matter diffusion constant which is water in our case. The parameters G, δ and Δ are controlled by us. The gyromagnetic ratio is defined by the protons quantum spin and hence we have no control over it. By multiplying it by the controllable parameters the equation can be simplified as

$$\frac{S}{S_o} = e^{-bD} \tag{3.2}$$

Further algebraic manipulation can lead us to the following form:

$$In(S) = In(S_o) - bD \tag{3.3}$$

We can see then that we can obtain a simple linear curve by plotting ln(S) on the Y-axis against b on the x-axis. This will form a straight line with a slope of -D and y-intercept of $In(S_o)$ as shown in the following figure.

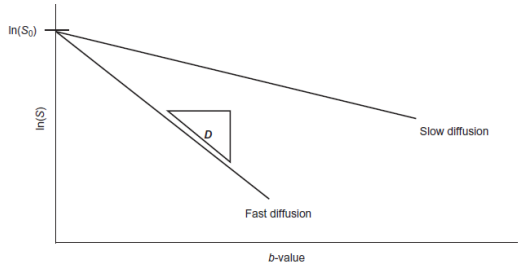

Figure 3.5: Relation between Signal Obtained from Diffusion and the Parameter b

3.2.4 Signal Loss VS Signal Intensity in Diffusion Measurement

Let is recall that the signal intensity at each pixel in the constructed image of a diffusion weighted experiment is affected by Proton Density (PD), T1 decay, T2* Decay and the water Diffusion. So If a certain pixel is more intense than another we can not be sure which of them is the certain cause. As mentioned before, we target diffused molecules by knowing if they have gained more phase or in other words caused more signal attenuation. To reduce the effect of T1, long TR is applied. A short TE will reduce the effect of T2* but also won't give enough time for diffusion caused phasing. That is we apply two experiments, not just for the usage of diffusion weighting gradient but to formulate the Diffusion constant in a ratio between the two experiments signals to drop the effect of the proton density and the Tw* decay.

Chapter 4

Diffusion Tensor Imaging

4.1 Diffusion Directionality

Diffusion in the human body usually has a preferred trajectory. Although that may seem as flow movement but the difference here lies in how we can describe them geometrically. Flowing water has a start and an end point and a single trajectory and can hence be described by a single vector. Diffusion on the other hand can only be described by a diffusion constant if it is isotropic. If it is anisotropic diffusion water flows in certain direction stronger than the others and can be described by the diffusion ellipsoid. The following figure illustrates this process.

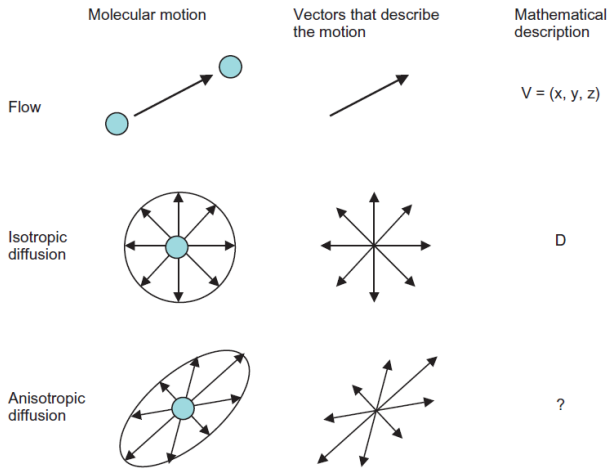

Figure 4.1: Flow VS Diffusion.
Image from Mori and Tournier (2014)

An ellipsoid is the most generic 3D shape that can be used to define anisotropic diffusion. To define an ellipsoid in the 3D space, we need 6 parameters: the length of each of the three principal axes and their orientations. the lengths are called $\lambda_1, \lambda_2, \lambda_3$ or eigen values and the orientations are described by three eigen vectors v_1, v_2, v_3. To obtain these six parameters we have to measure the Diffusion constant along six different directions.

4.2 Mathematics of Diffusion Tensor Imaging

In order to obtain the diffusion constant along 6 different directions we have to obtain 7 images. 6 of them are diffusion weighted with the a pair of diffusion weighting gradients along some direction and one is not weighted to obtain S_0. By applying a G_x we obtain an image of signal S_x sensitive to diffusion D_{xx} along the x direction. We can then calculate the diffusion constant along the x direction using the equation 3.2. By plugging S_x and D_xx:

$$\frac{S_x}{S_o} = e^{-bD_{xx}} \tag{4.1}$$

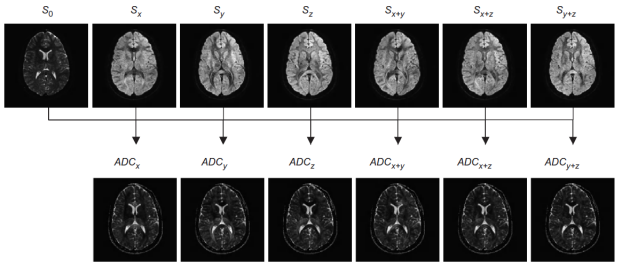

Figure 4.2: Flow VS Diffusion.
Image from Mori and Tournier (2014)

We can similarly solve for D_{yy} and D_zz. The other 3 directions will be the diagonals between the 3 principal axes so we obtain three signals S_{xy}, S_{xz} and S_{yz} by applying gradients along the direction of the the diagonals. In that case however we can not use the equation 3.2 as it is valid only for 1 dimensional diffusion. Applying a gradient G_{xy} produce a signal that is sensitive to both the x and y directions. So the diffusion constant along the diagonal XY for example will be equal to $\frac{1}{2D_{xx}} + D_{xy} + \frac{1}{2D_{yy}}$. Since we gave calculated D_{xx} and D_yy we can use the equation :

$$\frac{S_{xy}}{S_o} = e^{-b(\frac{1}{2D_{xx}} + D_{xy} + \frac{1}{2D_{yy}})} \tag{4.2}$$

Similarly we compute the terms D_z and D_{yz}. Now we can construct the so called **Diffusion Tensor** that is formulated as follows:

$$\begin{bmatrix} D_{xx} & D_{xy} & D_{xz} \\ D_{xy} & D_{yy} & D_{yz} \\ D_{xz} & D_{yz} & D_{zz} \end{bmatrix}$$

To obtain λ_1, λ_2, λ_3, v_1, v_2 and v_3 we perform diagonalization to the diffusion tensor and hence obtain the desired parameters as shown in the figure.

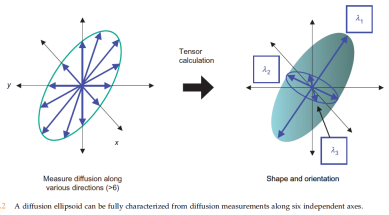

FIGURE 5.2 A diffusion ellipsoid can be fully characterized from diffusion measurements along six independent axes.

Figure 4.3: Flow VS Diffusion.
Image from Mori and Tournier (2014)

Chapter 5

Diffusion Kurtosis Imaging: The Enhanced Diffusion Tensor Imaging

5.1 Diffusion Kurtosis Imaging Origins

Diffusion kurtosis imaging (DKI) has emerged as a transformative extension of diffusion tensor imaging (DTI), offering unprecedented insights into tissue microstructure by quantifying the non-Gaussian behavior of water diffusion in biological systems. Unlike DTI, which assumes Gaussian diffusion, DKI measures the kurtosis of the diffusion probability distribution—a dimensionless parameter reflecting microstructural complexity through barriers, membrane interactions, and compartmentalization. This technique has demonstrated superior sensitivity in detecting pathological changes across neurological disorders, from traumatic brain injury (TBI) to high-grade gliomas, while overcoming critical limitations of conventional diffusion imaging in resolving crossing fibers and heterogeneous environments. Recent advancements, including sub-diffusion modeling frameworks, have further enhanced the clinical feasibility of DKI by enabling robust mean kurtosis estimation with reduced acquisition times. As DKI transitions from research to clinical practice, its ability to provide complementary biomarkers for disease stratification, treatment monitoring, and surgical planning positions it as a cornerstone of modern neuroimaging.

5.2 Theoretical Foundations of Diffusion Kurtosis Imaging

The diffusion of water molecules in biological tissues deviates significantly from the Gaussian behavior observed in homogeneous media due to structural barriers such as cell membranes, myelin sheaths, and extracellular matrix components. These microstructural features create restricted and hindered diffusion environments, leading to a probability distribution with heavier tails and sharper peaks than predicted by Brownian motion—a phenomenon quantified by the kurtosis parameter K.

The apparent kurtosis (K_{app}) is derived from the fourth-order expansion of the diffusion signal equation:

$$In(\frac{S_b}{S_o}) = -bD_{app} + \frac{1}{6}b^2D_{app}^2K_{app} \tag{5.1}$$

where S_b and S_o represent the diffusion-weighted and non-diffusion-weighted signals, respectively, and D_{app} is the apparent diffusion coefficient. Higher K_{app} values indicate greater microstructural complexity, as seen in white matter (K $\approx$ 1.0) compared to cerebrospinal fluid

($K = 0$).

DKI generates three primary metrics: the first is Mean Kurtosis (MK): The average kurtosis across all diffusion directions, sensitive to global microstructural heterogeneity. The second parameter is the Axial Kurtosis (AK) that is the Kurtosis parallel to the principal diffusion direction, influenced by axonal integrity and myelin content. Then comes Radial Kurtosis which is Kurtosis perpendicular to the principal direction, reflecting restrictions from cell membranes and myelin layers.

5.3 DKI vs. DTI in Clinical and Research Applications

5.3.1 Tractography and Crossing Fiber Resolution

DTI's inability to resolve crossing fibers within a voxel—the 'crossing fiber problem'—limits its accuracy in mapping complex white matter architectures. DKI addresses this by incorporating higher-order diffusion effects, enabling better angular resolution of fiber orientations. For example, q-ball imaging (QBI), a DKI-derived technique, resolves multiple intravoxel fiber directions using strong diffusion weighting ($b \geq 3000$ s/mm^2) and 60+ gradient directions, achieving tractography accuracy comparable to diffusion spectrum imaging (DSI) with shorter acquisition times. In brainstem and corpus callosum regions, DKI-based tractography reduces false-negative connections by 22–37% compared to DTI.

5.3.2 Disease Detection and Monitoring

DKI detects microstructural alterations missed by DTI in mild TBI patients. Grossman et al. found elevated MK in the thalamus and internal capsule of 22 TBI patients, correlating with cognitive impairment ($r = 0.68$, $p < 0.01$), whereas DTI metrics (FA, MD) remained normal. Animal models revealed subacute MK increases in contralateral cortex regions with reactive astrogliosis, suggesting DKI's sensitivity to secondary injury mechanisms.

In Alzheimer's disease (AD), DKI identifies early changes in the anterior corona radiata and prefrontal white matter, differentiating mild cognitive impairment (MCI) from controls with 89% accuracy. Parkinson's disease (PD) patients exhibit elevated MK in basal ganglia structures (+15%, $p < 0.05$), independent of disease severity, implicating preclinical microstructural disruption.

Multiple sclerosis (MS) studies demonstrate reduced MK in normal-appearing white matter (NAWM) regions, reflecting diffuse demyelination undetectable by conventional MRI. Yoshida et al. reported a 12% decrease in average MK across 24 NAWM ROIs in MS patients ($p < 0.05$), correlating with expanded disability status scale (EDSS) scores.

DKI outperforms DTI in distinguishing low-grade gliomas (LGGs) from high-grade gliomas (HGGs). Van Cauter et al. observed 40% higher MK in HGGs compared to LGGs ($p < 0.001$), while DTI-derived MD and FA showed no significant differences. Radial kurtosis (RK) proves particularly sensitive to infiltrative tumor margins, improving surgical resection planning.

5.4 Clinical Integration: When to Use DTI vs. DKI

DTI suffices for basic white matter mapping, stroke evaluation, and tumor ADC quantification and its shorter acquisition (5–10 minutes) suits emergency settings. when used with Lower b-values ($\leq$ 1000 s/mm^2) it maximized signal to noise ratio and provides less weight for motion artifacts. On the other hand, DKI is used for tumor grading, TBI evaluation, and neurodegenerative disease staging. DKI also is suitable for advanced tractography as preoperative planning for epilepsy or tumor surgery benefits from DKI's crossing fiber resolution. Recent advancements, such as the sub-diffusion model, reduce DKI acquisition times to potentially less than 4 minutes while maintaining diagnostic accuracy, narrowing the practicality gap with DTI.

5.5 Limitations

DKI's reliance on high b-values ($\geq$ 2000 s/mm^2) increases susceptibility to noise and geometric distortions. Multi-shell acquisition protocols and denoising algorithms, as implemented in the Human Connectome Project, mitigate these issues but require specialized hardware. When it comes to clinical validation, prospective multi-center studies are needed to standardize DKI metrics across scanner platforms. The Connectome 1.0 dataset provides a normative reference for MK (0.87 ± 0.22 in white matter) but pathological thresholds remain institution-specific.

References

Assaf, Y. and Basser, P. J. (2005), 'Composite hindered and restricted model of diffusion (charmed) mr imaging of the human brain', *NeuroImage* **27**(1), 48–58.

Assaf, Y. and Cohen, Y. (2000), 'Assignment of the water slow-diffusing component in the central nervous system using q-space diffusion mrs: Implications for fiber tract imaging', *Magnetic Resonance in Medicine* **43**(2), 191–199.

Assaf, Y. and Pasternak, O. (2007), 'Diffusion tensor imaging (dti)-based white matter mapping in brain research: A review', *Journal of Molecular Neuroscience* **34**(1), 51–61.

Assaf, Y., Pianka, P., Rotshtein, P., Sigal, M. and Hendler, T. (2003), 'Deviation of fiber tracts in the vicinity of brain lesions: Evaluation by diffusion tensor imaging', *Israel Journal of Chemistry* **43**(1–2), 155–163.

Basser, P. J. (1995), 'Inferring microstructural features and the physiological state of tissues from diffusion-weighted images', *NMR in Biomedicine* **8**(7), 333–344.

Basser, P. J., Mattiello, J. and LeBihan, D. (1994), 'Mr diffusion tensor spectroscopy and imaging', *Biophysical journal* **66**(1), 259–267.

Basser, P. J. and Pierpaoli, C. (1996), 'Microstructural and physiological features of tissues elucidated by quantitative-diffusion-tensor mri', *Journal of Magnetic Resonance, Series B* **111**(3), 209–219.

Basser, P. J. and Pierpaoli, C. (1998), 'A simplified method to measure the diffusion tensor from seven mr images', *Magnetic resonance in medicine* **39**(6), 928–934.

Bozzali, M. (2002), 'White matter damage in alzheimer's disease assessed in vivo using diffusion tensor magnetic resonance imaging', *Journal of Neurology, Neurosurgery Psychiatry* **72**(6), 742–746.

Catani, M. and ffytche, D. H. (2005), 'The rises and falls of disconnection syndromes', *Brain* **128**(10), 2224–2239.

Clark, C. A., Barrick, T. R., Murphy, M. M. and Bell, B. A. (2003), 'White matter fiber tracking in patients with space-occupying lesions of the brain: A new technique for neurosurgical planning?', *NeuroImage* **20**(3), 1601–1608.

Duke University (2023), 'Mri: The dance of the whirling protons'.
URL: *https://sites.duke.edu/apep/module-3-alcohol-cell-suicide-and-the-adolescent-brain/explore-more/mri-the-dance-of-the-whirling-protons/*

Exchange, P. S. (2019), 'Why do some protons align against the magnetic field?', Online forum post.
URL: *https://physics.stackexchange.com/questions/484043/why-do-some-protons-align-against-the-magnetic-field*

Jensen, J. H., Helpern, J. A., Ramani, A., Lu, H. and Kaczynski, K. (2005), 'Diffusional kurtosis imaging: The quantification of non-gaussian water diffusion by means of magnetic resonance imaging', *Magnetic Resonance in Medicine* **53**(6), 1432–1440.

Kanaan, R. A. et al. (2005), 'Diffusion tensor imaging in schizophrenia', *Biological Psychiatry* **58**(12), 921–929.

MATLAB1 (2023), 'Review: Magnetic resonance imaging (mri)', *MATLAB1 Articles* .
URL: *https://matlab1.com/review-magnetic-resonance-imaging-mri/*

Mori, S. and Tournier, J.-D. (2014), *Introduction to Diffusion Tensor Imaging and Higher Order Models*, 2 edn, Elsevier, Amsterdam.

Moseley, M. E. et al. (1990), 'Diffusion-weighted mr imaging of anisotropic water diffusion in cat central nervous system', *Radiology* **176**(2), 439–445.

Pajevic, S. and Pierpaoli, C. (1999), 'Color schemes to represent the orientation of anisotropic tissues from diffusion tensor data: Application to white matter fiber tract mapping in the human brain', *Magnetic Resonance in Medicine* **42**(3), 526–540.

Papadakis, N. G. et al. (1999), 'A study of rotationally invariant and symmetric indices of diffusion anisotropy', *Magnetic Resonance Imaging* **17**(6), 881–892.

Papadakis, N. G. et al. (2002), 'Study of the effect of csf suppression on white matter diffusion anisotropy mapping of healthy human brain', *Magnetic Resonance in Medicine* **48**(2), 394–398.

Pierpaoli, C., Jezzard, P., Basser, P. J., Barnett, A. and Di Chiro, G. (1996), 'Diffusion tensor mr imaging of the human brain', *Radiology* **201**(3), 637–648.

Sakuma, H. et al. (1991), 'Adult and neonatal human brain: Diffusional anisotropy and myelination with diffusion-weighted mr imaging', *Radiology* **180**(1), 229–233.

Westin, C.-F. et al. (2002), 'Processing and visualization for diffusion tensor mri', *Medical Image Analysis* **6**(2), 93–108.

Witwer, B. P. et al. (2002), 'Diffusion-tensor imaging of white matter tracts in patients with cerebral neoplasm', *Journal of Neurosurgery* **97**(3), 568–575.